Supplementary Figure Legends

Figure S1. The hair regeneration cycle is altered as mice age.
A 12 month old mouse was photographically documented for 358 days until it died naturally. Mouse age (days) is indicated above each photograph. The hair wave propagation distance in 12 month old mice reduces with age from young (14 months, from day 431 to 454) to "middle aged" status (17 months, from day 513 to 526) to almost no propagation in old mice (24 months, day 681 to 688), which results in smaller hair cycle domains.

Figure S2. Hair regeneration cycle in 24-26 month old mice.
The hair regeneration cycle of 24 month old mice was followed until the mice died naturally 57 days later. Most hair cycle domains remained in telogen. Even though some anagen initiation can occur, the regeneration cycle domains are all small (n=5).

Figure S3. Hair regeneration cycle in young mice.
In young mice, the telogen period is short and the regeneration cycle domains are big.

Figure S4 "Telogen retention" in old mice is rescued when small skin grafts were transplanted onto a young macro-environment.
When a small skin graft (5x3 mm) from an old mouse was transplanted onto young SCID skin, hair growth and telogen retention were rescued. The hair wave in the secondary cycle (day 89 post transplantation) propagated into the surrounding young skin as well as throughout the skin graft.

Figure S5. "Telogen retention" persisted in the central part of a large skin graft from an old mouse.
When a large skin graft (15x10 mm) from an old mouse was transplanted to a young SCID mouse, the HFs from the graft regenerated completely during the first cycle (from day 26 post transplantation). However, this round of regeneration may be due to wound healing in response to engraftment surgery. In the secondary cycle (from day 51 post transplantation), hair growth and telogen retention were partially rescued in peripheral parts of the transplant, which showed a shortened telogen period as seen in young adult mice, while the central part of the transplant remained unchanged from that of the donor skin. We also found that the hair wave of the secondary cycle propagated only into the host tissue but not to the center of the donor tissue (day 51 and 61 post transplantation). Moreover, at later times (day 107 post transplantation), the small central hair cycle domain could not propagate to the surrounding area. This

is similar to what was seen for the original donor mouse skin.

Figure S6. Only peripheral part can be rescued when large old skin was transplanted.
Another example demonstrates that large old skin transplant can totally regenerated during the first cycle after transplantation (day 25 post transplantation). However, during the 2nd (day 69 post transplantation) and 3rd (day 127 post transplantation) regeneration cycle, only peripheral part of the transplants can enter anagen phase and central part of the transplant remains in "telogen retention" status.

Figure S7. Old environment inhibits hair regeneration of young skin.
One small piece of young skin taken from 6-month-old mouse was transplanted onto the back of 24-month-old mouse. The regeneration response of the young skin was inhibited and the telogen period was prolonged. (red circle: the transplant area)

Figure S8. The expression pattern of Wnt signaling pathway members, *Bambi*, *Sostdc1*, and *Fgf-7*, in 6 month old adult C57BL/6 mice.
In situ hybridization showed that Wnt family members were expressed as follows: Wnt3a, inner root sheath; Wnt5a, both inner and outer root sheath; Wnt6, mainly in outer root sheath; Lef-1, dermal papilla as well as both the inner and outer root sheath. Bambi is located in the dermal papilla and outer root sheath area; Sostdc1 and Fgf-7 are only expressed in the dermal papilla.

Figure S9. The expression pattern of the Wnt signaling pathway in 24 month old mice is not altered.
Whole mount in situ hybridization of skin samples taken from a 24 months old mouse containing different phases of the hair regeneration cycle revealed that the Wnt signaling pathway, including Wnt5a, Wnt6, and β-catenin, are activated in the hair germ and outer root sheath during propagating and autonomous anagen phases but not during refractory telogen phase.

Figure S10. Dermal inhibitors *Bmp2, Dkk1* and *Sfrp4* are highly expressed in 24-month-old mice

Whole mount in situ hybridization of skin samples taken from 24 month old mice shown as a skin strip (a) and magnification of follicles (b). Different phases of the hair regeneration cycle are shown in colored boxes. *Bmp2* and Wnt signaling pathway inhibitors, including *Dkk1* and *Sfrp4*, were negative during the propagating anagen

phase of young mice (Plikus et al., 2011). They are expressed in old mice here. c. d. No staining can be identified in all stages when sense probes of *Bmp2*, *Dkk1*, *Sfrp4* were used on the skin samples taken from the same 24 month old mice. Panel b is also shown in Fig. 3a.

Figure S11. Hair wave propagator follistatin is down-regulated in 24 month old mice

a. Whole mount in situ hybridization in 6 month old mouse shows that, outside of the follicle, *follistatin* is expressed in P and C phases but not R and A phases. Different phases of the hair regeneration cycle are shown in colored boxes. b. The expression of *follistain* is down-regulated in 24 month old mouse even during propagating phase. Panel a is also shown in Fig. 4a and panel b is also shown in Fig. 4g.

Figure S12. Periodic expression of cyclic *follistatin* is out of phase with the BMP cycle.

a. Whole mount in situ hybridization of a skin strip from 6 month old mouse containing different stages of the hair cycle revealed that follistatin was up-regulated during propagating anagen and competent telogen but not during autonomous anagen and refractory telogen. This expression pattern is out of phase with the BMP cycle which is expressed only during autonomous anagen and refractory telogen but not during propagating anagen and competent telogen. b. Double staining of follistaitn and perilipin-A.

Figure S13. Histological morphology of the hair follicles after waxing.

H&E staining of the skin sample taken from 6 month old young mice at different time points after hair waxing revealed that HFs starts to extend and anagen is initiated 4 days after waxing.

Figure S14. Expression of *follistatin* and PDGFA after synchronized waxing.

a. After waxing-induced hair regeneration, macro-environmental *follistatin* is highly upregulated at 12 hours but PDGFA is not induced until 4 days, when anagen is initiated. b. Hairs that regenerate from the transplantation margin could propagate in both directions, to the old skin transplant and to the young host. Compared to the increased expression of *follistatin* in old skin transplants, the expression of BMP-2 is down-regulated. Panel b is also shown in Fig. 2d.

Figure S15. Follistatin can initiate anagen and induce hair wave propagation.

a. Anagen occurs 13 days after insertion of follistatin soaked beads and propagated to surrounding skin at day 17, reaching its maximum area of about 250 mm^2 at day 22. b. albumin containing PBS-soaked beads showed no anagen re-entry even after 42 days. (red arrow: beads insertion area). Panel a and b are also shown in Fig. 4d and 4e.

Figure S1.

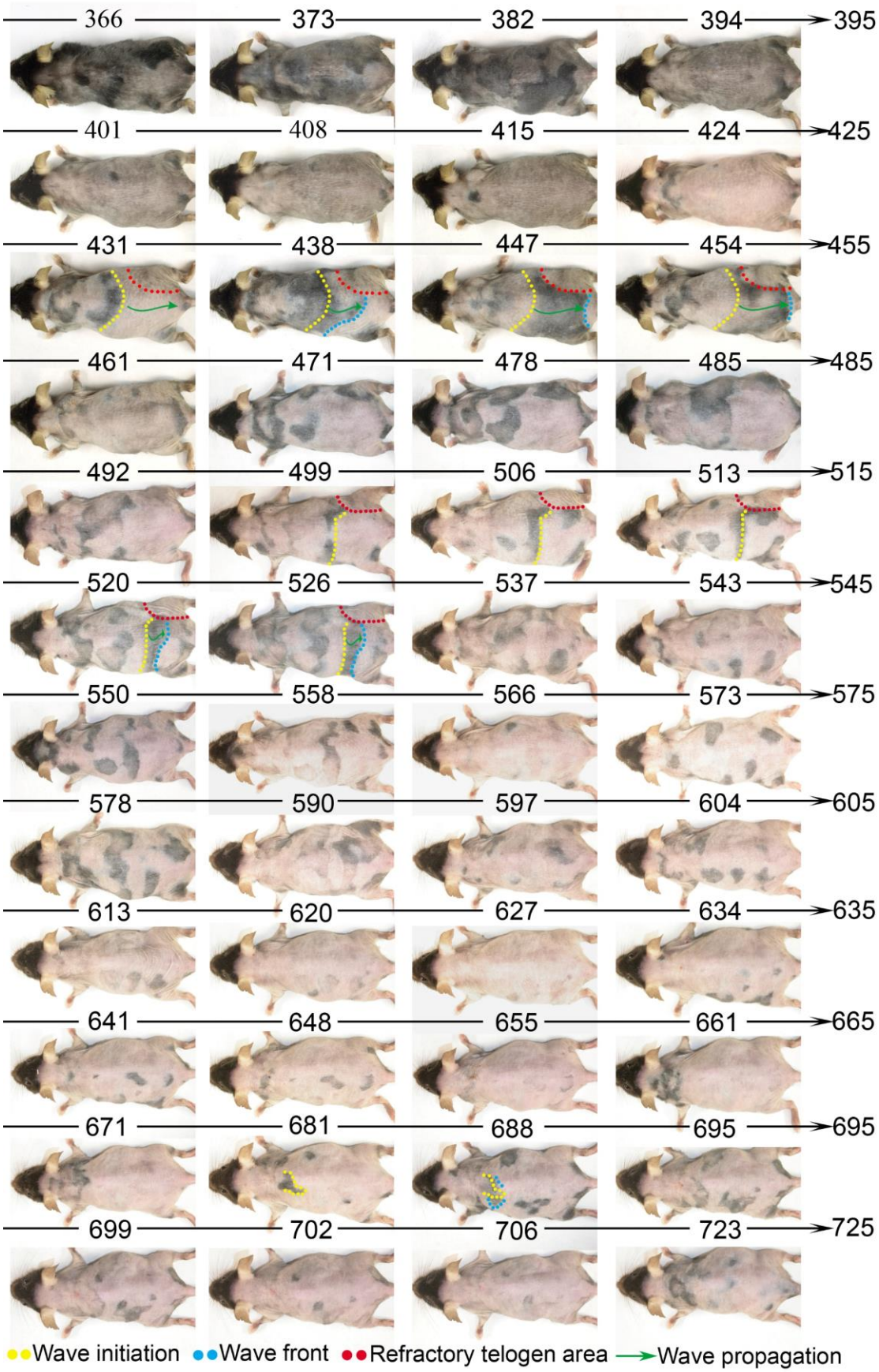
366
373
382
394
395
401
408
415
424
425
431
438
447
454
455
461
471
478
485
485
492
499
506
513
515
520
526
537
543
545
550
558
566
573
575
578
590
597
604
605
613
620
627
634
635
641
648
655
661
665
671
681
688
695
695
699
702
706
723
725
Wave initiation
Wave front
Refractory telogen area
Wave propagation

Figure S2.

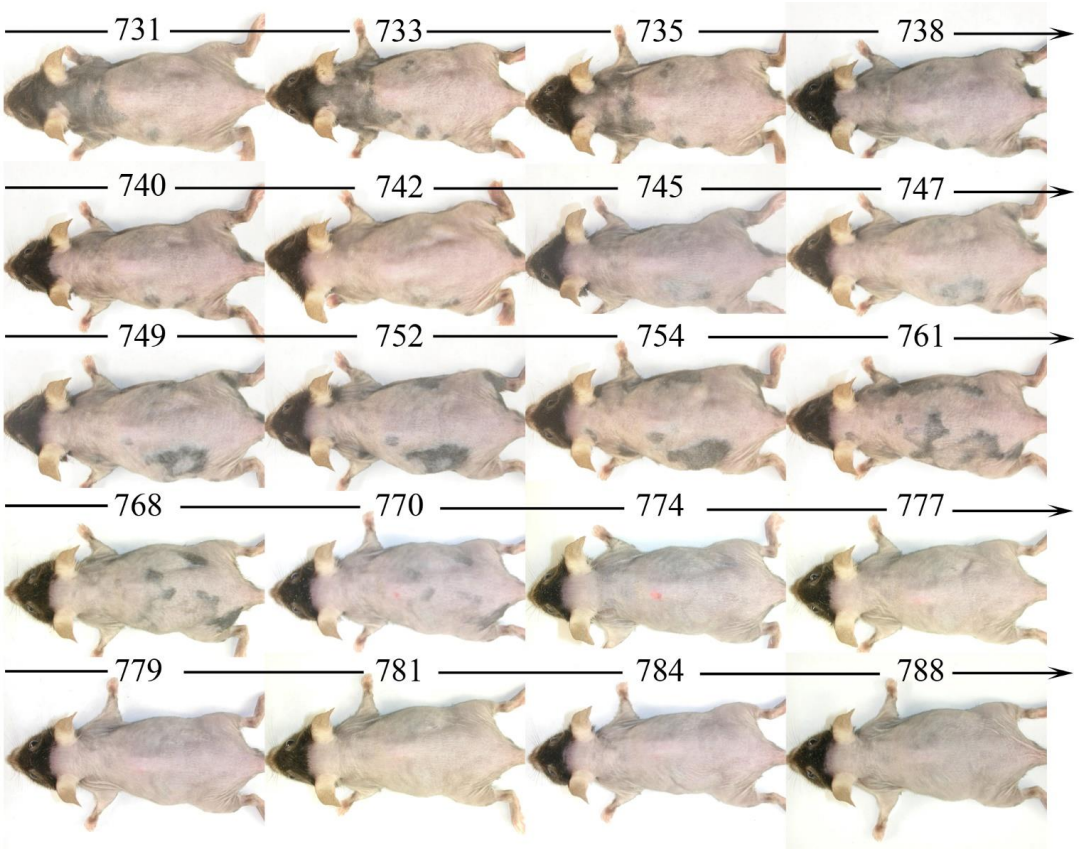
731
733
735
738
740
742
745
747
749
752
754
761
768
770
774
777
779
781
784
788

Fighre S3.

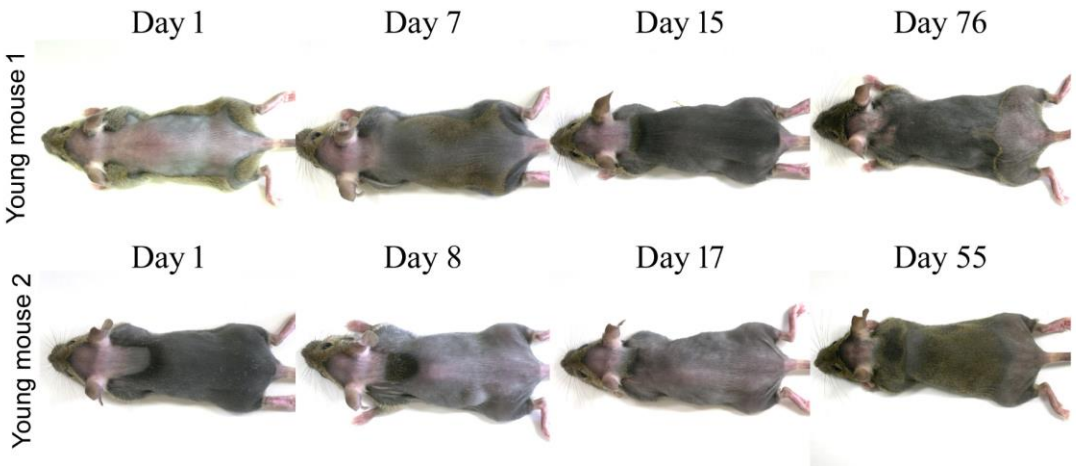
Day 1
Day 7
Day 15
Day 76
Young mouse 1
Day 1
Day 8
Day 17
Day 55
Young mouse 2

Figure S4.

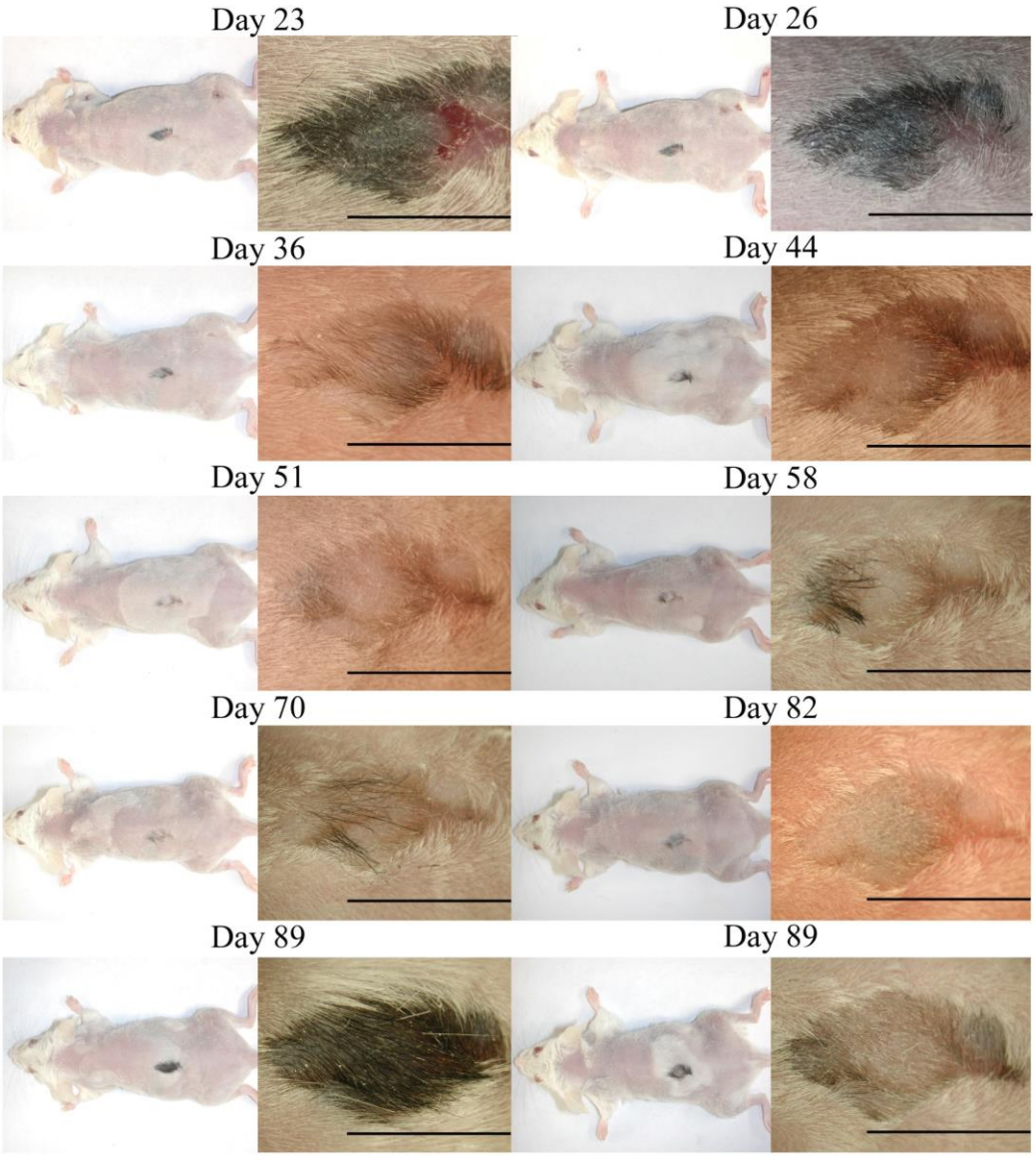
Day 23
Day 26
Day 36
Day 44
Day 51
Day 58
Day 70
Day 82
Day 89
Day 89

Figure S5.

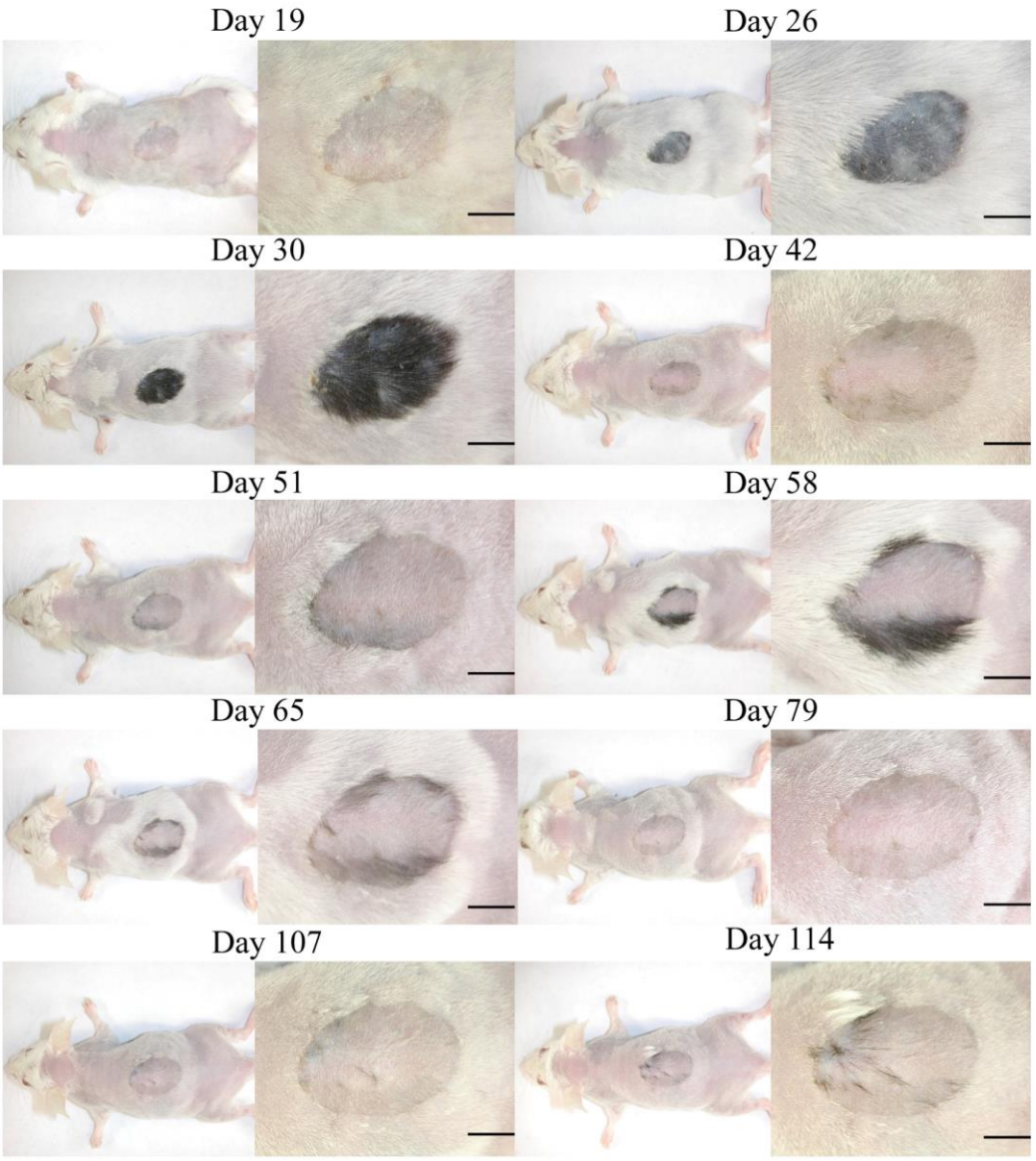
Day 19
Day 26
Day 30
Day 42
Day 51
Day 58
Day 65
Day 79
Day 107
Day 114

Figure S6.

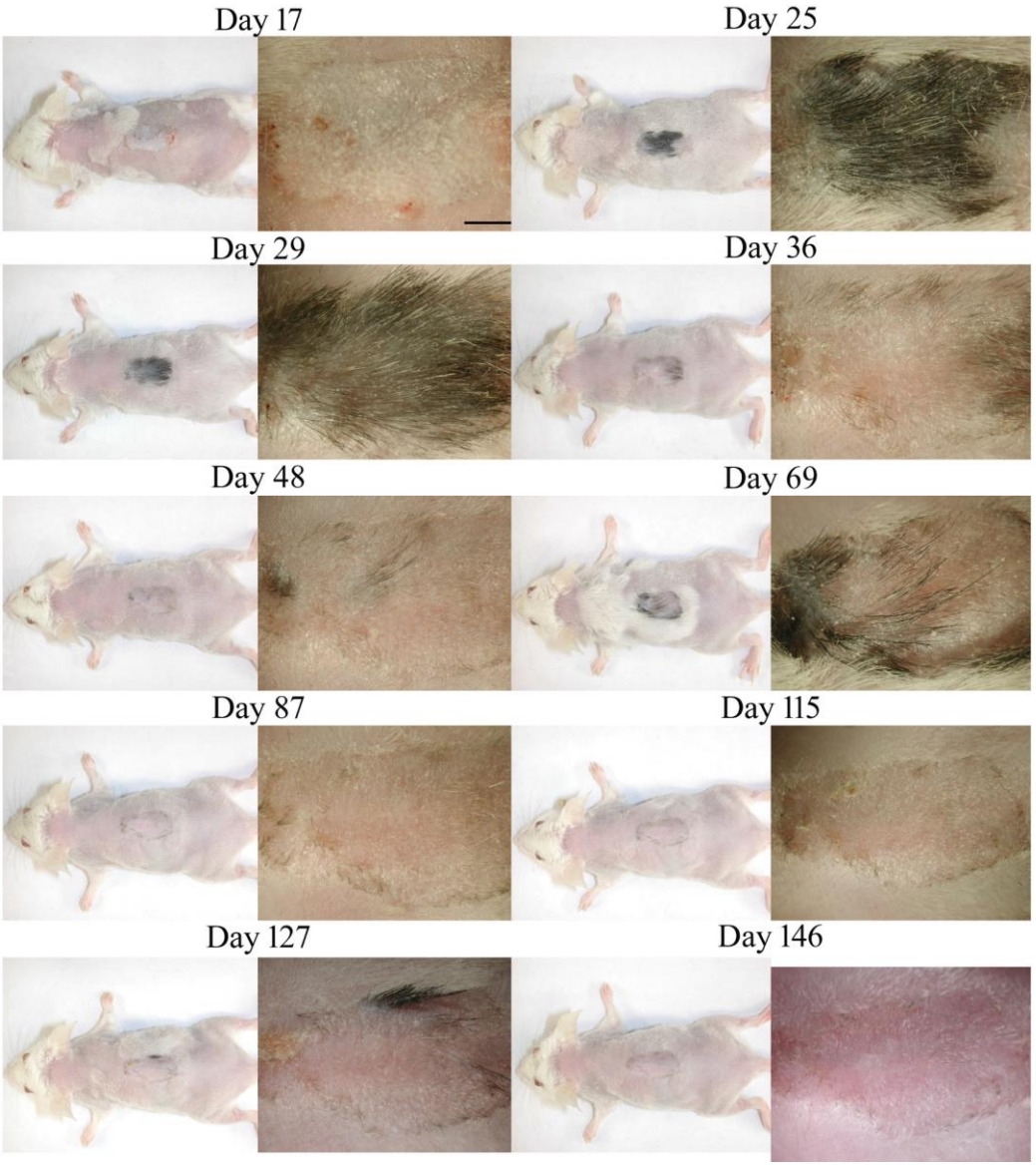
Day 17
Day 25
Day 29
Day 36
Day 48
Day 69
Day 87
Day 115
Day 127
Day 146

Figure S7.

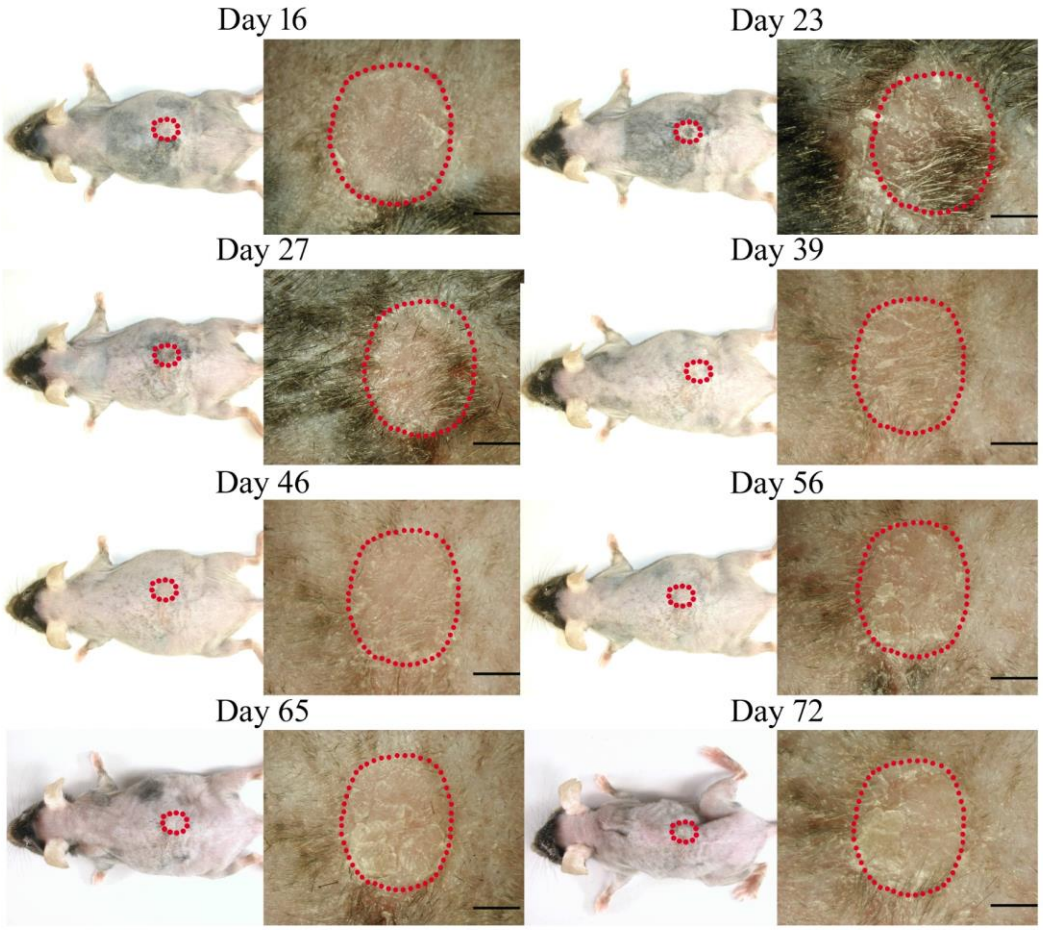

Figure S8.

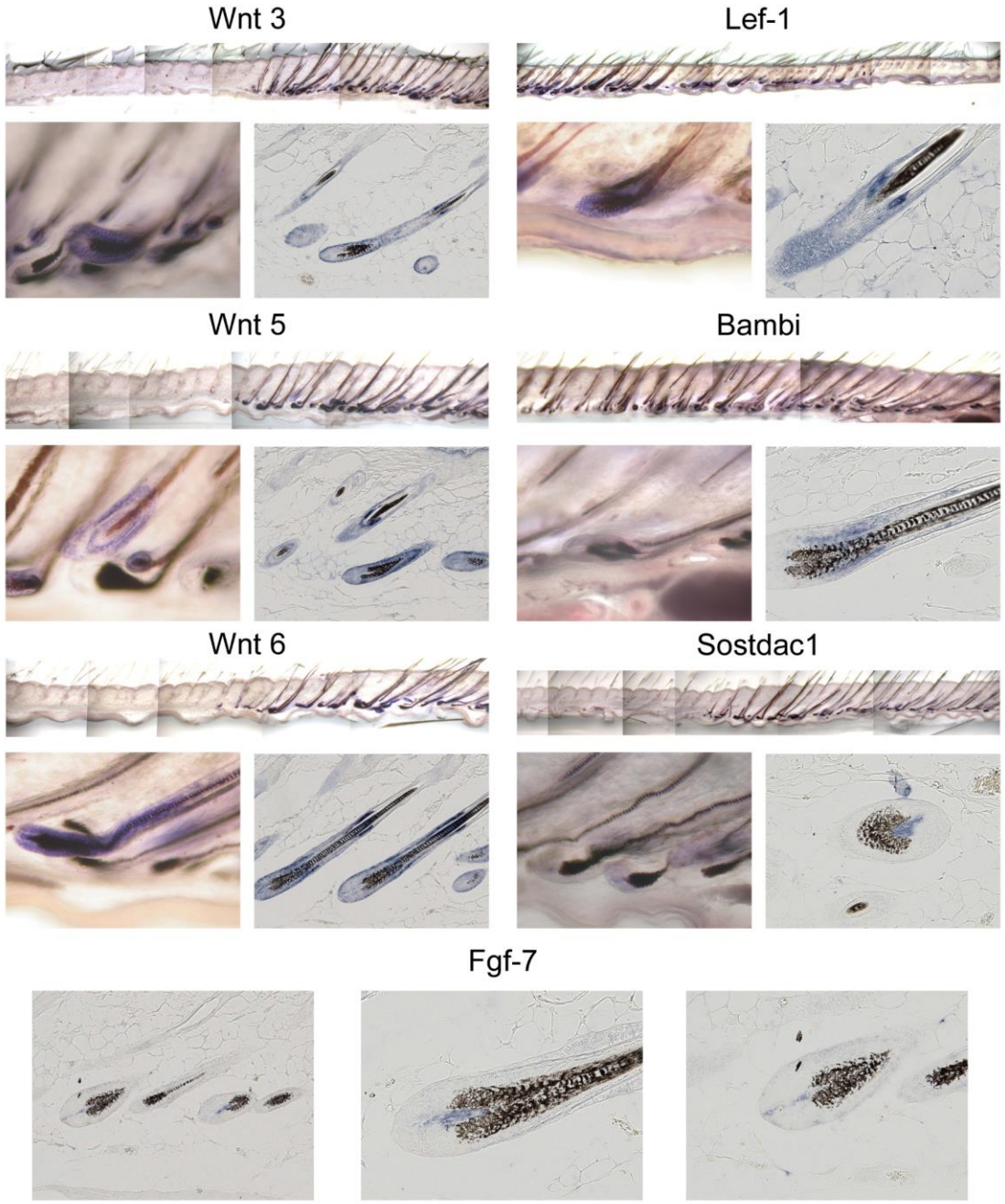

Figure S9.

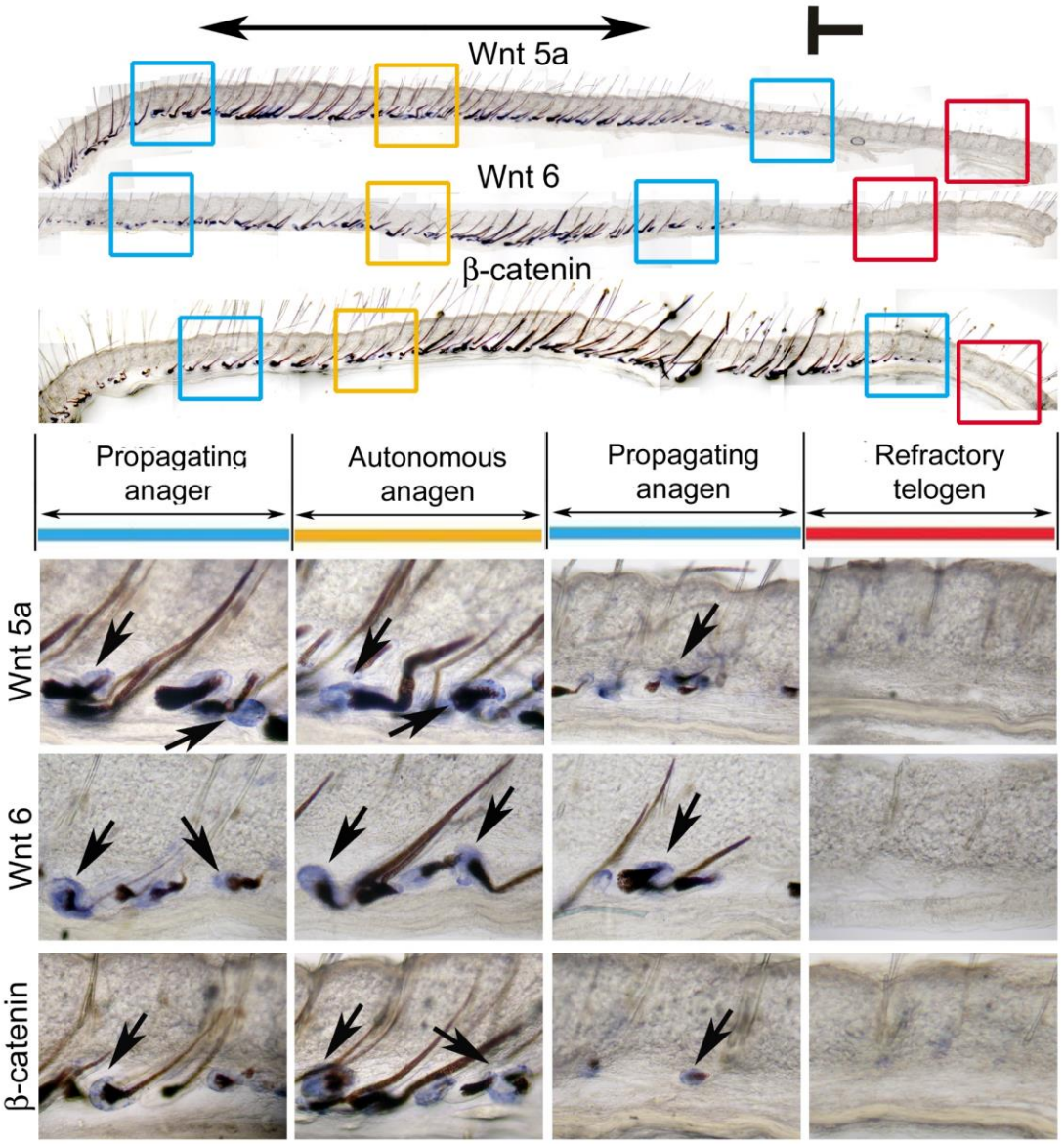
Wnt 5a
Wnt 6
β-catenin
Propagating anager
Autonomous anagen
Propagating anagen
Refractory telogen
Wnt 5a
Wnt 6
β-catenin

Figure S10.

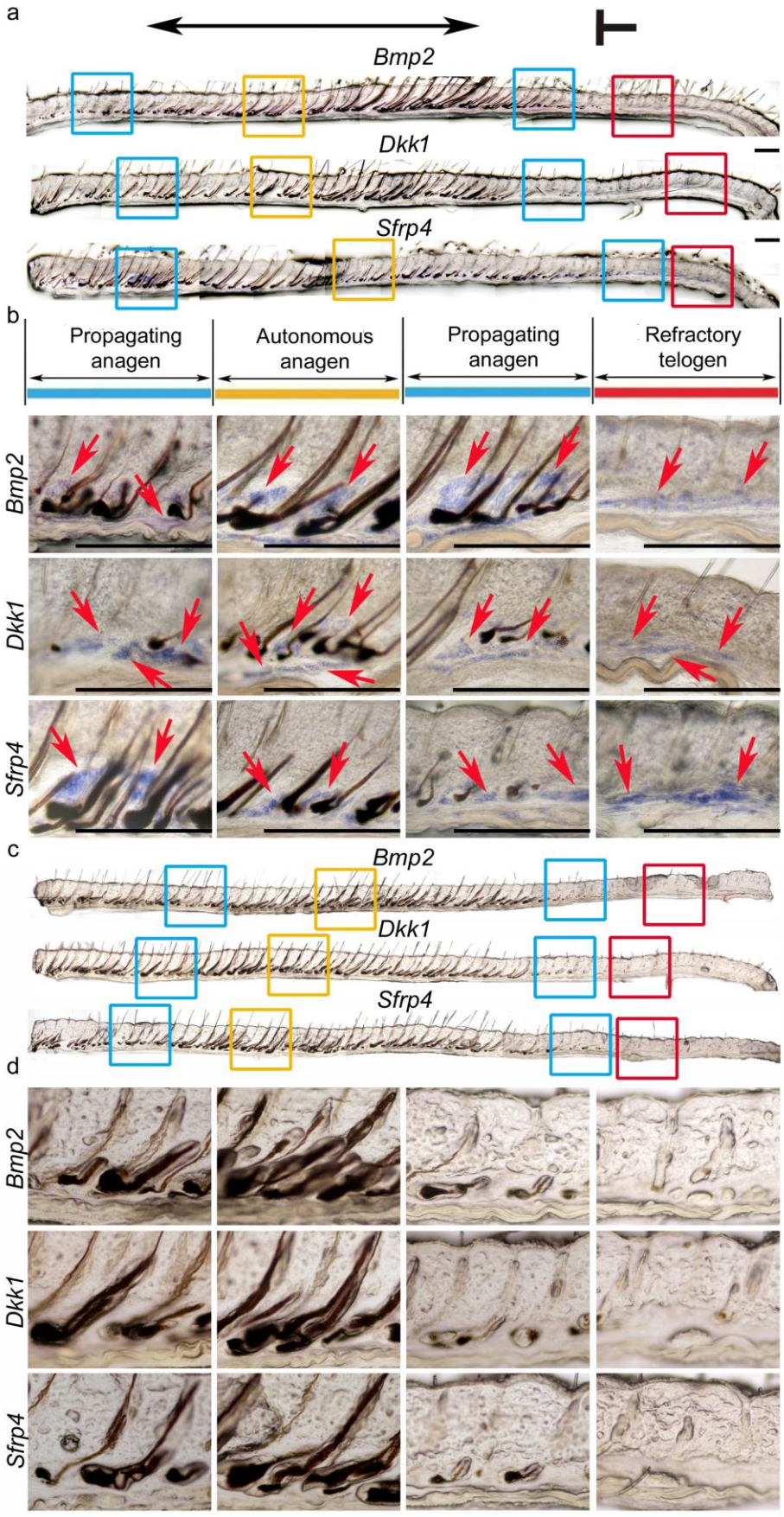
a
Bmp2
Dkk1
Sfrp4
b
Propagating anagen
Autonomous anagen
Propagating anagen
Refractory telogen
Bmp2
Dkk1
Sfrp4
c
Bmp2
Dkk1
Sfrp4
d
Bmp2
Dkk1
Sfrp4

Figure S11.

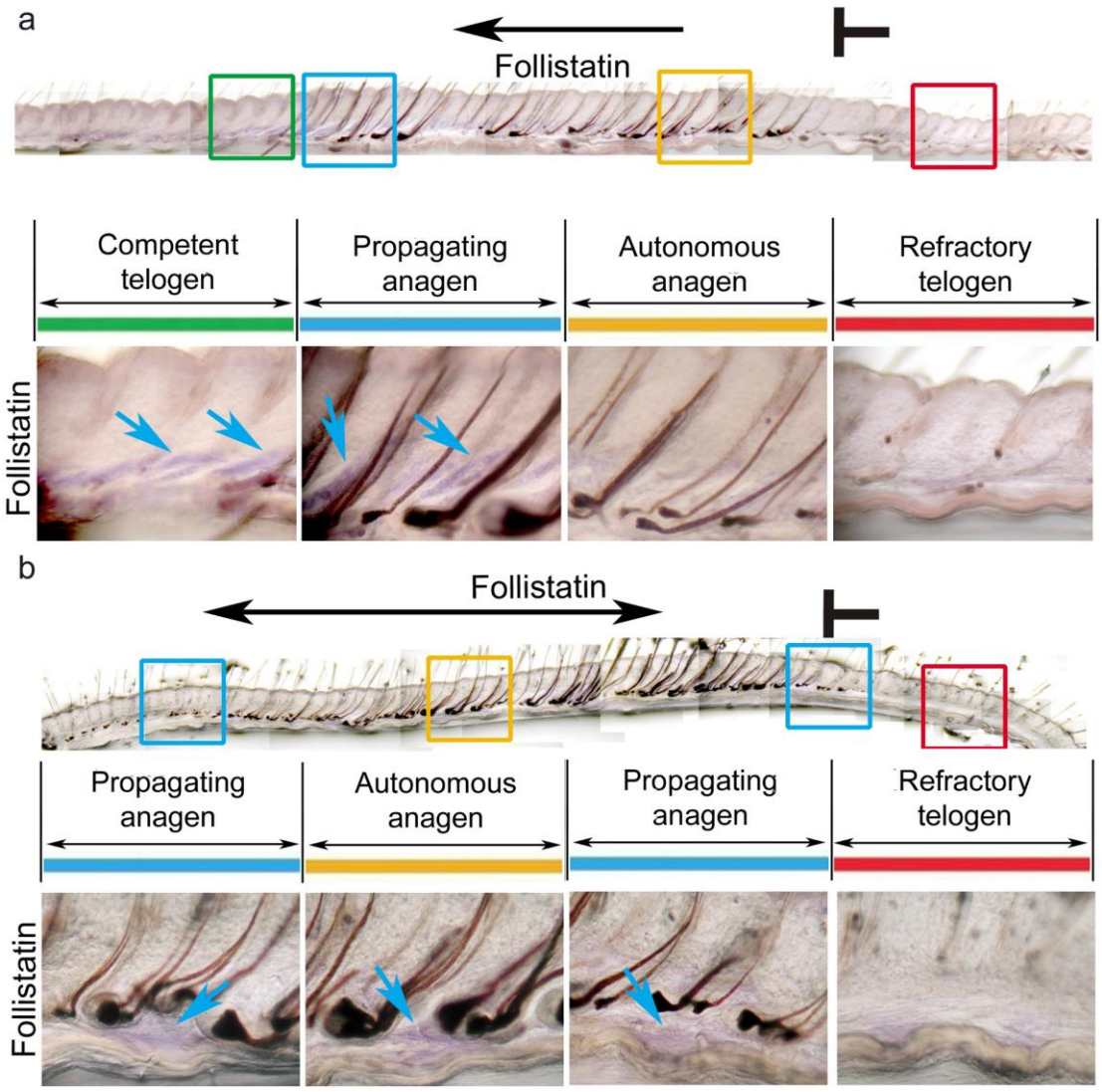
a
Follistatin
Competent telogen
Propagating anagen
Autonomous anagen
Refractory telogen
Follistatin
b
Follistatin
Propagating anagen
Autonomous anagen
Propagating anagen
Refractory telogen
Follistatin

Figure S12.

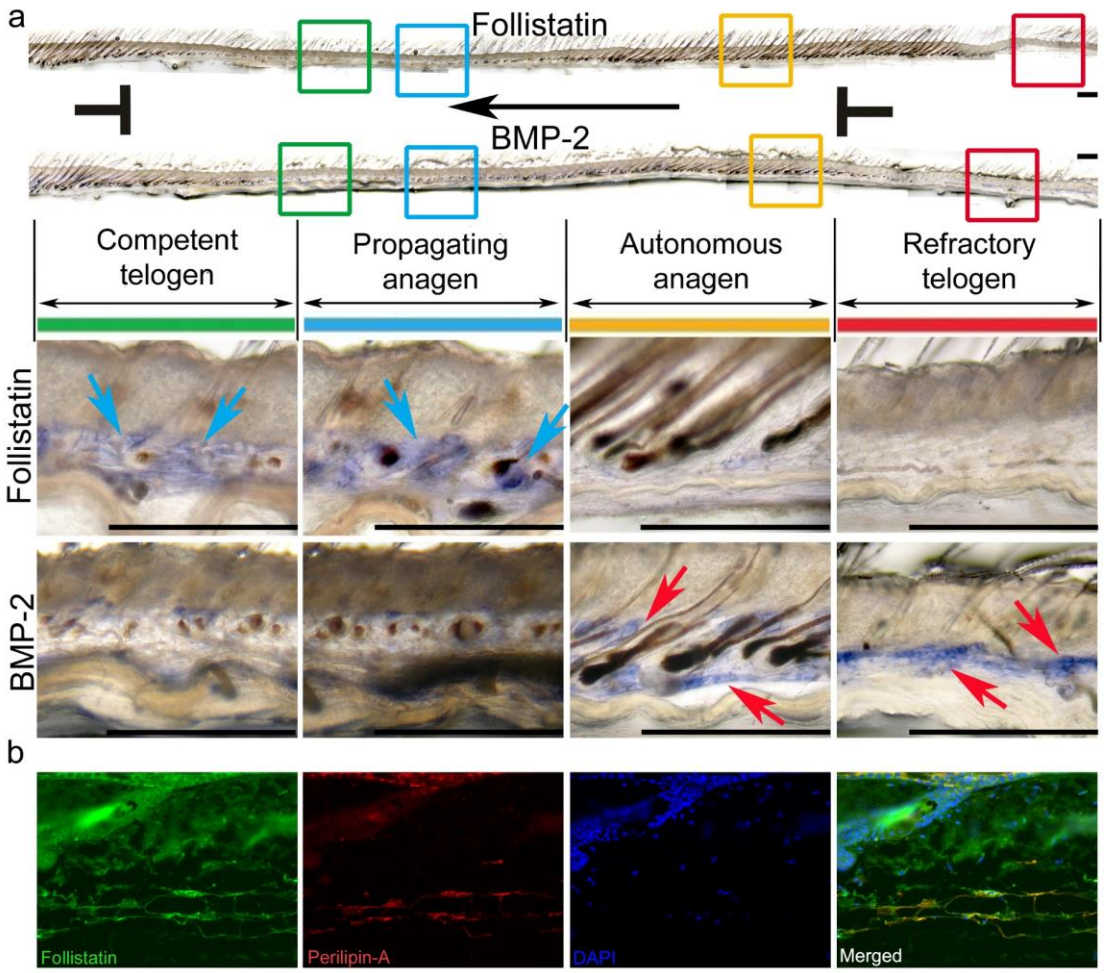
a
Follistatin
BMP-2
Competent telogen
Propagating anagen
Autonomous anagen
Refractory telogen
Follistatin
BMP-2
b
Follistatin
Perilipin-A
DAPI
Merged

Figure S13.

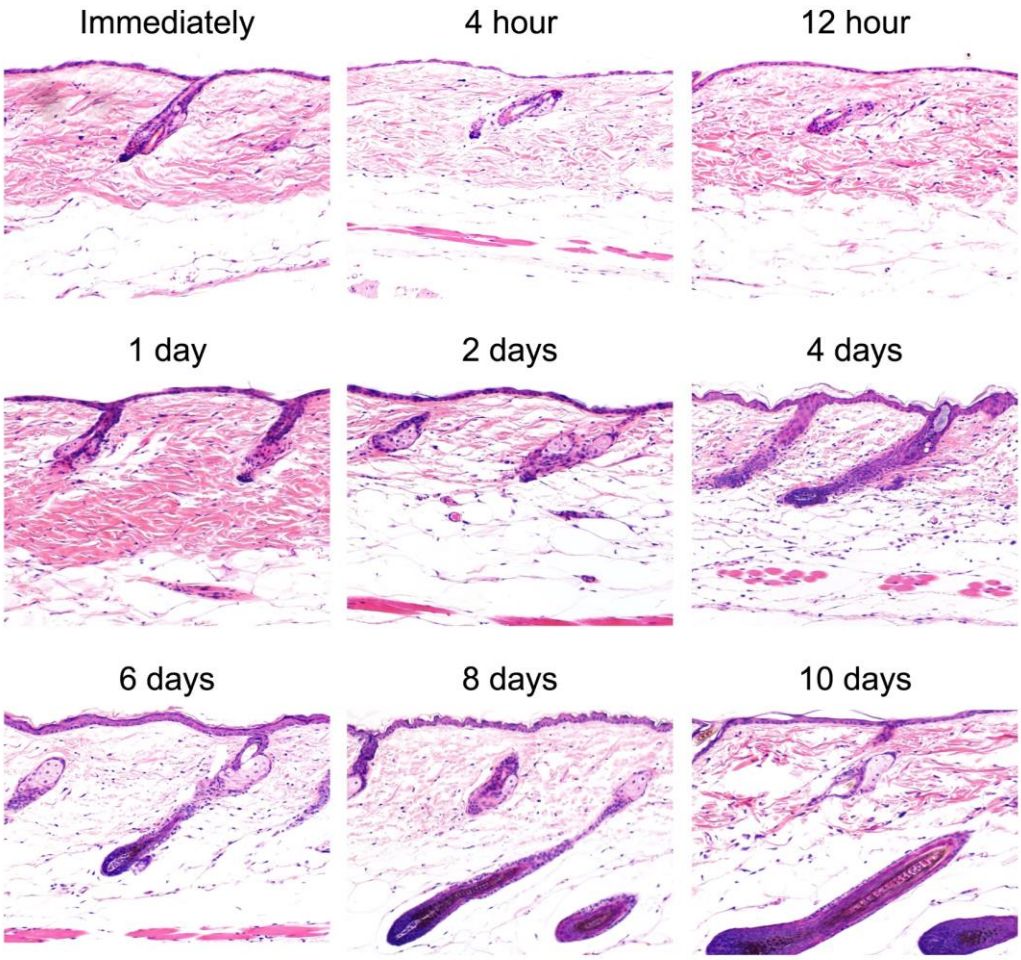
Immediately
4 hour
12 hour
1 day
2 days
4 days
6 days
8 days
10 days

Figure S14.

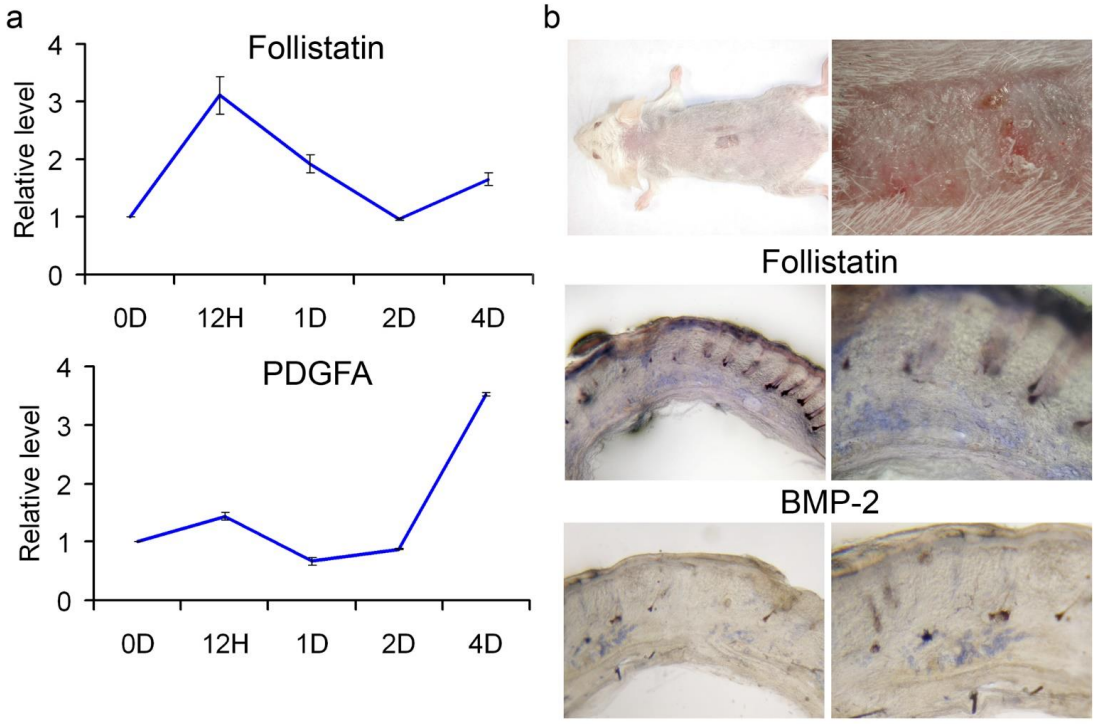
a
Follistatin
Relative level
4
3
2
1
0
0D
12H
1D
2D
4D
PDGFA
Relative level
4
3
2
1
0
0D
12H
1D
2D
4D
b
Follistatin
BMP-2

Figure S15.

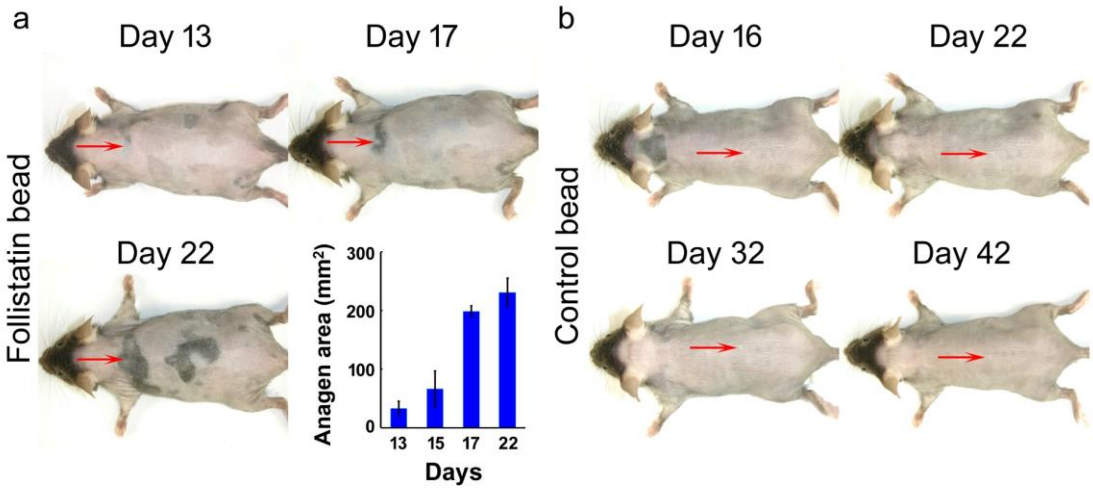
a
Day 13
Day 17
Follistatin bead
Day 22
Anagen area (mm²)
300
200
100
0
13
15
17
22
Days
b
Day 16
Day 22
Control bead
Day 32
Day 42

Supplementary table

Table S1. Primer Pairs Used for Quantitative Real-Time RT-PCR

Target genes	Primer	Sequence
Follistatin	forward	5’-TGCCTGCTCTTCTGGCGTGC-3’
	reverse	5’-CCGTTTCTTCCGAGATGGAGTTGC-3’
Bmp2	forward	5’-AGCAAGGACGTCGTGGTGCC-3’
	reverse	5’-CTCCACGGCTTCTTCGTGATGGA-3’
Dkk1	forward	5’-CGGGCTCTGCTGTCAGTGTGG-3’
	reverse	5’-AGCGCAAGGGTAGGGCTGGTA-3’
Sfrp4	forward	5’-TGAGCCCTGATCGGTGCAAGTG-3’
	reverse	5’-GCAACCACTCCTCTGGACGGC-3’
GAPDH	forward	5’-GGGAAGCCCATCACCATCT-3’
	reverse	5’-CGGCCTCACCCCATTTG-3’

Mathematical model

While multiple different pathways have been shown to activate or inhibit follicle growth, the precise molecular interactions that regulate the hair follicle cycle are not currently well quantified. This lack of detailed molecular understanding means that it is not currently feasible to build a model in which the expression of particular genes are modelled in explicit detail. Instead we consider a model with a single generic activator and inhibitor that we define to represent the overall expression of activators and inhibitor pathways, respectively. Although the proposed model does not explicitly describe molecular expression in hair follicles, it does provide a theoretical framework which can explain how observations made on different scales might be causally related.

Recap

In the proposed model [3] a combination of positive and negative feedback loops in the activator/inhibitor dynamics give a single follicle an emergent property of excitability and the functional phases of the hair follicle cycle (anagen, refractory telogen and competent telogen) are emergent phenomena. We define the activities of an activator, $v(t)$, and an inhibitor, $w(t)$, and propose a two variable, FitzHugh-Nagumo-like model [1] with governing equations given by

$$\varepsilon \frac{\partial v}{\partial t} = f(v) - av - bw + I + D_A \nabla^2 v + \xi(t), \quad (1)$$

$$\frac{\partial w}{\partial t} = cv - dw + J, \quad (2)$$

where ε is a small parameter that separates slow and fast time scales in the governing dynamics, $f(v)$ is the activation rate, a and d are natural decay rates, b and c are cross inhibition and activation rates, I and J are background rates of activator and inhibitor activation, respectively, $\xi(t)$ represents a zero-correlated noise defined such that $\langle \xi(t)\xi(t-t') \rangle = 2\Gamma\delta(t-t')$ and D_A is the activator diffusion coefficient. The parameters I, J, a, b, c and d are positive constants. We consider a caricature of excitable dynamics in which the activator dynamics are given by the piece-wise linear function [2]

$$f(v) = \begin{cases} \alpha_1 v & \text{if } v < v_0; \\ \alpha_1 v_0 + \alpha_2(v - v_0) & \text{if } v_0 < v < v_1; \\ \alpha_1 v_0 + \alpha_2(v_1 - v_0) & \text{if } v_1 < v. \end{cases} \quad (3)$$

We assume that the constants α_1, α_2, v_0 and v_1 are positive and that the linear activator production rate switches at the threshold activator level v_0 from the rate α_1 to α_2. At the threshold activator value v_1, the production attains the maximal rate $\alpha_1 v_0 + \alpha_2(v_1 - v_0)$. When such production dynamics are coupled with linear decay, the net rate of self-activation takes a cubic-lie form (assuming $0 < \alpha_1 < a < \alpha_2$). The follicle cycle can be understood as follows: a follicle has a stable steady-state in which activator and inhibitor activities are low. The steady-state is stable to small perturbations but a sufficiently large perturbation can 'excite' a follicle such that the activator enters a transient state, corresponding to anagen, where activator activity becomes high. As anagen proceeds the inhibitor is slowly activated and eventually its level reaches a threshold which forces the follicle to enter telogen, where activator is switched off but inhibitor remains high. Refractory telogen is the time taken for the inhibitor to decay and the follicle to return to steady-state while competent telogen represents the time a follicle spends at steady state before it gets re-excited. Hence the excitable medium description of the follicle growth can naturally account for the functional phases of the hair cycle (see Figure 7 in the Main Text).

In Figure 1 we present numerical solutions of equations (2). Note the stochastic excitation leading to a propagating wave of high activator activity. In Murray et al. [3] we present a detailed description of model behavior.

Figure 1: Propagation of single waves after spontaneous activation. Activator (top row) and inhibitor (bottom row) activities are plotted at a sequence of times in a two-dimensional spatial domain. Equations (1) and (2) were solved as described in Murray et al. [3].

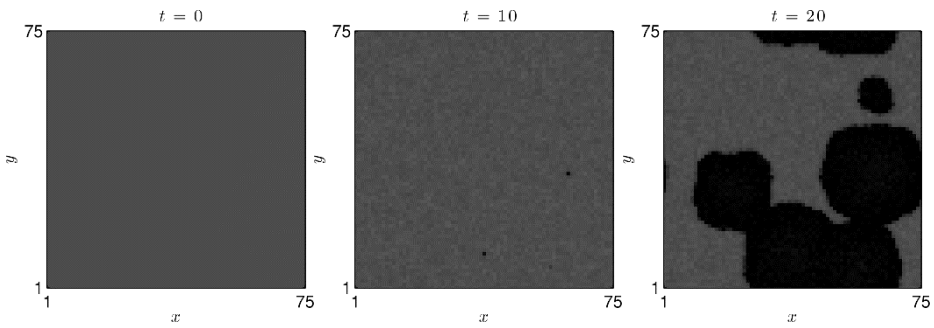

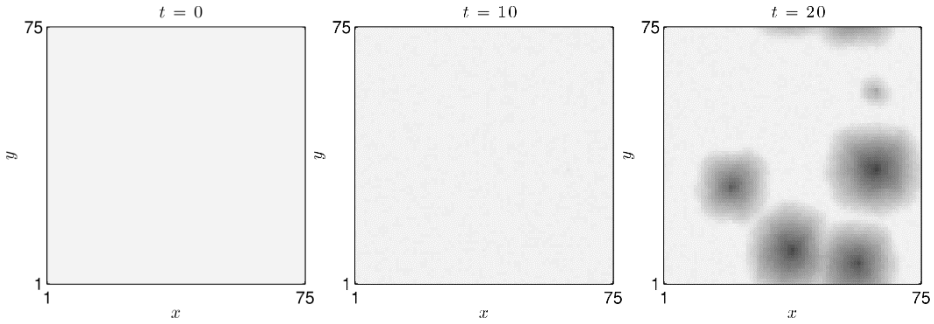

Application to observations in aging mice

The phenomenon of competent telogen arises in the model as a consequence of the of the stochastic term: a follicle at steady-state is perturbed by the stochastic term. Eventually, a sufficiently large stochastic perturbation can kick it far enough away from equilibrium such that it becomes excited. We can approximate the mean time for such an excitation to occur and find that

$$T_C \sim \frac{2\pi}{\sqrt{-\Phi''(v_{ss})\Phi''(v_{thr})}} \exp\left(\frac{\Phi(v_{thr})-\Phi(v_{ss})}{\Gamma}\right), \qquad (4)$$

where $\Phi(v_{ss})$, $\Phi(v_{thr})$ are the effective potential energies when the follicle is in the steady state and threshold states, respectively, and primes denote differentiation (see Murray et al. [3] for further details). Hence, (4) can be used to describe how parameters representing molecular phenomena can be related to competent telogen times. In Figure 8 (a) and (b) of the Main Text we demonstrate how the length of telogen increases with inhibitor production rate and decreases with activation rate. Hence our model is consistent with the hypothesis that increased inhibitor production in aging mice results in more stable follicles and longer telogen times.

We can also use equations (2) to determine how the speed of wave propagation varies with changes to model parameters and thus relate observations of tissue scale (the propagating wavefront) and molecular phenomena. Although we have not derived an explicit expression for the wave speed, we have calculated the numerical solution of equations (1) and (2) for a wavefront propagating in one spatial dimension and in Figures 8 (c) and (d) of the Main Text we illustrate how this quantity changes with model parameters. We find that the wavefront velocity decreases with increased inhibitor and decreased activator expression rates. Hence our model supports the

hypothesis that observed molecular changes in ageing mice yield the phenomenon of decreased wave speeds and hence smaller domain sizes.

References

[1] Fitzhugh R (1961) Impulses and physiological states in theoretical models of nerve membrane. Biophys J 1: 445–466

[2] McKean HP (1970) Nagumo's equation. Adv Math 4: 209–223

[3] Murray PJ, Plikus MV, Maini PK, Choung CM, Baker RE (2012) Modelling hair follicle growth dynamics as an excitable medium. PLoS Comp Bio 8(12):e1002804

[4] Plikus MV, Mayer JA, de La Cruz D, Baker RE, Maini PK, et al. (2008) Cyclic dermal BMP signalling regulates stem cell activation during hair regeneration. Nature 451: 340–344.

[5] Plikus MV, Baker RE, Chen CC, Fare C, de la Cruz D, et al. (2011) Self-organizing and stochastic behaviors during the regeneration of hair stem cells. Science 332: 586–589